

ORIGINAL INNOVATION

Open Access



# Dynamic performance of simply supported girder bridges subjected to successive earthquake-tsunami events

Ruiwei Feng<sup>1</sup>, Deming Zhu<sup>1</sup> and You Dong<sup>1,2\*</sup> 

\*Correspondence:  
you.dong@polyu.edu.hk

<sup>1</sup> Department of Civil and Environmental Engineering, The Hong Kong Polytechnic University, Hung Hom, Kowloon, Hong Kong, China

<sup>2</sup> Research Institute for Sustainable Urban Development, The Hong Kong Polytechnic University, Hong Kong, China

## Abstract

Coastal bridges are susceptible to severe damage when subjected to successive earthquake-tsunami events. Previous studies mainly consider the tsunami loadings as hydrodynamic forces, whereas other hydrodynamic forces such as uplift and slamming forces, are not fully investigated. Moreover, there are limited studies on the dynamic performance of simply supported girder bridges under the earthquake-tsunami sequences. To this end, this paper aims to conduct an in-depth investigation on dynamic performance of simply supported bridges subjected to sequential earthquake and tsunami hazards by means of a high-fidelity wave force simulation approach. More specifically, a typical, already constructed simply supported girder bridge is taken as the example bridge, and the numerical model of this bridge is built using the analytical platform OpenSees. The applied time series of tsunami wave force with five wave heights are generated based on a refined computational fluid dynamics (CFD) model, and are separately combined with the time histories of 21 pairs of far-field earthquake records to generate the sequential earthquake and tsunami loadings. Subsequently, nonlinear time history analyses (NTHAs) are carried out to obtain the structural dynamic responses, and the effects of preceding earthquakes and wave heights on the performance are investigated. Results indicate that the bearings are susceptible to the damage in the longitudinal direction of the bridge under the sequential earthquake and tsunami loadings, while the piers sustain more damage in the transverse direction. The preceding earthquakes have a significant effect on the bridge performance, and the effect becomes more pronounced with the increase of the ground motion intensity. The contribution of the tsunami loadings to the bridge response increases as the wave height rises. In particular, the transverse pier drift is dominated by the tsunami loadings when the wave height is higher than 7 m. The outcome of this study could aid the design and management of coastal bridge subjected to successive earthquake-tsunami events.

**Keywords:** Successive earthquake-tsunami events, Dynamic response, Simply supported girder bridges, Computational fluid dynamics, Preceding earthquakes, Wave height

## 1 Introduction

An offshore earthquake event could produce a sudden displacement of the water surface and in turn trigger a tsunami (Clague et al. 2003). In the past two decades, massive sequential earthquake-tsunami events occur worldwide, such as the 2004 Indian Ocean tsunami, 2010 Chile tsunami, and 2011 Great East Japan (Tohoku) tsunami (Goda et al. 2015, 2021), which lead to catastrophic consequences to coastal infrastructures. Particularly, as a crucial part of littoral transportation networks, coastal bridges are susceptible to noticeable damage (Gidaris et al. 2017). Therefore, a growing number of studies have been carried out to investigate the performance of coastal structures under the cascading earthquake and tsunami hazards.

Reliable numerical analysis and damage evaluation approaches are the premises of structural performance assessment (Tu et al. 2019; Gautam and Dong 2018). For this purpose, relevant studies have been conducted for the structures under sequential earthquake and tsunami loadings. Taking the fully dynamic case as the benchmark, Rossetto et al. (2019) proposed that the combination of an earthquake nonlinear response history analysis, a free vibration and a tsunami variable depth pushover analysis can achieve preferable predictions for the structural responses. Park et al. (2012) put forward a two-stage analysis procedure to derive the collapse fragility of a light-frame wood building. Attary et al. (2021) developed a physics-based method for estimating the risk of structures considering the correlation between the earthquake and the tsunami. Apart from the proposed analysis procedures and assessment methods, recent studies also focus on the structural behavior under the successive earthquake and tsunami events, especially on the effect of prior earthquakes on the overall structural performance. Petrone et al. (2020) compared the fragilities of a reinforced concrete frame subjected to tsunami inundation only, and under sequential earthquake and tsunami loadings. Results indicate that the preceding earthquakes have a small effect on the tsunami fragility. Similarly, on the basis of a reinforced concrete wall building, Tagle et al. (2021) reported that the structural capacity is not affected by the previous earthquake damage before the concrete crushing in the critical sections. Moreover, Ji et al. (2021) investigated the response of single-degree-of-freedom (SDOF) structures under the earthquake-tsunami loadings, and they found that earthquake-tsunami loadings are able to enlarge the inelastic displacement ratio compared to only sustaining the seismic actions.

The above-mentioned studies mainly take the buildings as case-studies, however, the studies on the performance assessment of bridges under the multi-hazard of tsunamis following earthquakes are in infancy. Among the existing studies, Akiyama and Frangopol (2014) investigated the reliability of bridges under the seismic and tsunami hazards. They reported that additional attentions are needed to guarantee the tsunami resistance of bridges. Carey et al. (2019) quantified the impact of sequential earthquake and tsunami hazards on the soil-foundation-bridge (SFB) systems. Results demonstrate that the resistance of the SFB system to the tsunami loadings reduces due to the preceding earthquake motions. Additionally, Xu et al. (2021b) developed the joint multi-hazard fragility curves for a reinforced concrete (RC) box-girder bridge under the successive earthquake-tsunami events. Their results show that the preceding earthquake motions impose a significant effect on the bridge tsunami fragility for lower damage states, whereas has a minor impact on the tsunami fragility at extensive and complete damage

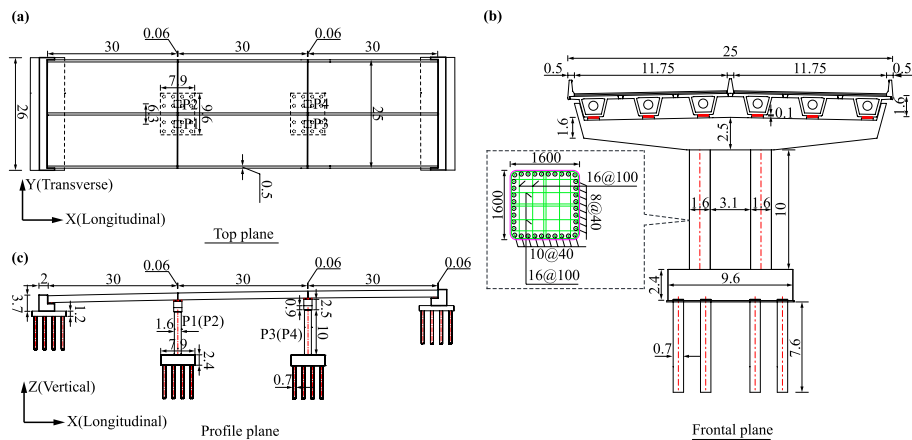


**Fig. 1** General configuration of the prototype bridge (unit: m): **a** top plane, **b** frontal plane and **c** profile plane

levels. Despite the progress made in these studies, the tsunami loadings on structures focus on the hydrodynamic forces during steady-flow conditions and are applied to the bridges through the nonlinear static analysis (i.e., pushover analysis). The hydrostatic and buoyant forces, the impulsive surge forces, and other hydrodynamic forces such as uplift and slamming forces, which are significant to the structural performance (FEMA 2012), are not fully considered. Hence, further refinements for the simulation of tsunami forces are necessitated. Moreover, previous studies mainly take the continuous girder bridge as the prototype bridge, however, very limited research is conducted on the simply supported girder bridges that have sustained severe damage during the historical successive earthquake and tsunami hazards (Sugimoto and Unjoh 2007; Salem et al. 2016).

Given the research gaps, this paper aims to explore the dynamic performance of simply supported bridges under sequential seismic and tsunami loadings. A typical simply supported concrete girder bridge is selected as the example bridge. Then, refined tsunami inundation time histories are generated from an advanced three-dimensional computational fluid dynamics (CFD) model, and are combined with a wide range of ground motion time series to form a suite of earthquake-tsunami pairs. Finally, the response histories under the cascading earthquake and tsunami loadings are obtained, and the effects of the preceding earthquake and the tsunami wave height on the bridge performance are assessed.

## 2 Bridge description and the numerical model

### 2.1 Overview of the prototype bridge

A typical three-equal-span simply supported girder bridge is taken as the case-study bridge. Figure 1 shows the general configuration of the prototype bridge. The deck consists of six precast RC box-section girders with a total length of 30 m and a height of 1.6 m. Expansion joints with an initial gap of 0.06 m are set between the decks, as well as between the decks and the abutments. The interior span is supported on two-pier bents, and the clear lateral spacing between two piers is 3.1 m. Each pier has a total height of 10 m, and is constructed with 1.6 m × 1.6 m square cross-sections. The outer ends of the exterior spans are founded on the abutments which have a width of 26 m and a height

of 3.7 m. The 0.75 m × 0.75 m laminated rubber bearings with the rubber layer thickness of 0.1 m are employed, and their top and bottom steel plates are anchored to the superstructure and the substructure, respectively. Moreover, the abutments and the piers are erected on 9.6 m × 7.9 m rectangular RC pile caps, and a group of 16 0.7 m diameter piles with a height of 7.6 m are designed beneath each pile cap. In addition, the deck and the cap beam comprise Chinese Grade C50 concrete (MOT (Ministry of Transport) 2018). The piers are constructed using the Chinese Grade C40 concrete, reinforced using 40 mm diameter Chinese Grade HRB400 longitudinal bars and 16 mm diameter HRB400 transverse bars with a vertical spacing of 0.1 m. The foundations are made of Chinese Grade C35 concrete.

### 2.2 Numerical modelling procedure

The numerical model of the prototype bridge is built by means of the OpenSees (McKenna 2011). Figure 2 illustrates the modeling details. The deck is simulated using the elastic beam-column element. The overall weight of the deck is considered as the sum of each nodal mass calculated based on the cross-sectional properties of the corresponding elements. In particular, the pounding effect of the deck is captured through the zero-length element with an impact material developed from the Hertz contact model (Muthukumar and DesRoches 2006) (Fig. 2(a)). The laminated rubber bearings are modeled using the zero-length element with elastic uniaxial material (MOT (Ministry of Transport) 2020), as illustrated in Fig. 2(b). Due to the symmetry in the transverse direction, three bearings on one side can be merged into one bearing. Therefore, a total of

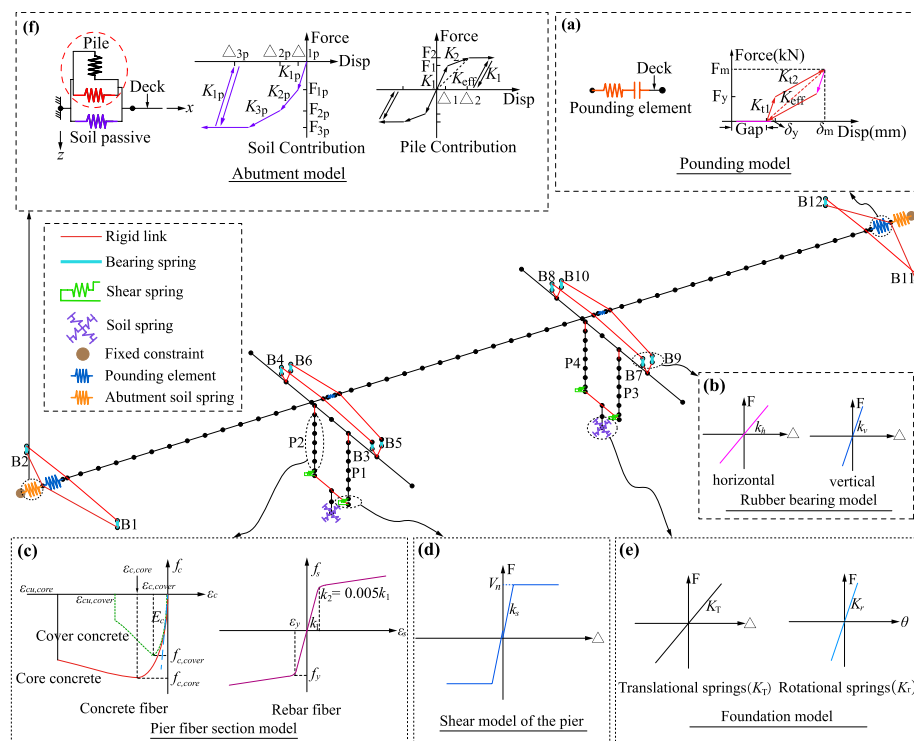


**Fig. 2** Numerical modelling details of the case-study bridge: **a** pounding effect, **b** rubber bearing, **c** pier fiber section, **d** horizontal shear model of the pier, **e** effects for the pier bents and **f** SSI effects for the abutment

12 bearings (two bearings in a row) are built in the numerical model. The horizontal ( $k_h$ ) and vertical stiffness ( $k_v$ ) of the merged bearings are obtained according to Eqs. (1) (MOT (Ministry of Transport) 2020) and (2) (MOT (Ministry of Transport) 2007):

$$k_h = \frac{3GA_b}{t_b} \quad (1)$$

$$k_v = \frac{3\alpha A_b GS^2}{t_b} \quad (2)$$

where  $G$ ,  $A_b$  and  $t_b$  are the shear modulus, plan area and the rubber layer thickness of each bearing in the prototype bridge, respectively,  $\alpha$  is the constant factor that is dominated by the geometric and boundary conditions of the bearing, and  $S$  is the shape factor. The piers are built using the displacement-based beam-column elements with fiber cross-sections. As shown in Fig. 2(c), the stress-strain relationship for the confined and unconfined concrete fibers are defined by the *Concrete04* material (Mander et al. 1988), while the *Steel02* material (Taucer et al. 1991) is utilized to describe the constitutive relationship of reinforcing bars. Due to the loading pattern of tsunami waves, the pier may fail in shear (Xu et al. 2021a, b). Therefore, the shear failure is considered in the numerical modelling of piers. Specifically, the shear response of the pier is captured by 6-degree-of-freedom (6-dof) zero-length elements at the pier bottom. The horizontal shear behavior is simulated employing the elastic-perfectly plastic material (Xu et al. 2021b) (Fig. 2(d)), and its initial stiffness ( $k_s$ ) is calculated according to LeBorgne and Ghannoum (LeBorgne and Ghannoum 2014) as:

$$k_s = \frac{E_c \cdot A_g}{3L} \quad (3)$$

where  $E_c$  is the elastic modulus of concrete,  $A_g$  and  $L$  are the gross section area and the clear length of the pier, respectively. The shear strength ( $V_n$ ) is obtained based on the Priestly et al. (Priestly et al. 1994). For the vertical and rotational stiffness, large stiffness is adopted to ensure that very small deformations are produced. The pile caps are mimicked using the elastic beam-column elements with lumped translational masses assigned to the corresponding nodes. Moreover, the soil-structure interaction (SSI) effect for the pier bents (Fig. 2(e)) are accounted for using zero-length elements with 6-dof elastic uniaxial materials, and their stiffness is determined based on Mangalathu et al. (2018). For the SSI effect of the abutment region (Fig. 2(f)), zero-length elements with hysteretic material are adopted to simulate its complex performance in the translational directions, as per the study of Nielson (2005).

### 3 Generation of earthquake-tsunami sequences

#### 3.1 Ground motions

To comprehensively reflect the seismic performance of the bridge, a wide range of ground motion records should be chosen (Feng et al. 2018, 2021). In this study, 21 far-field ground motions records (42 individual horizontal components) with different site and source characteristics, as well as epicentral distances are selected from the ATC-63 project report (FEMA P695) (ATC 2008), as listed in Table 1. It is worth noting that

**Table 1** Summary of the information regarding the selected earthquake records

No.	RSN	Year	Event name	Recording station	Magnitude	Epicentral distance (km)
1	68	1971	San Fernando	LA - Hollywood Stor	6.61	39.49
2	125	1976	Friuli, Italy	Tolmezzo	6.5	20.24
3	169	1979	Imperial Valley	Delta	6.53	33.73
4	174	1979	Imperial Valley	El Centro Array #11	6.53	29.53
5	721	1987	Superstition Hills	El Centro Imp. Co.	6.54	35.83
6	725	1987	Superstition Hills	Poe Road (temp)	6.54	11.2
7	752	1989	Loma Prieta	Capitola	6.93	9.78
8	767	1989	Loma Prieta	Gilroy Array #3	6.93	31.4
9	848	1992	Landers	Coolwater	7.28	82.12
10	900	1992	Landers	Yermo Fire Station	7.28	85.99
11	953	1994	Northridge	Beverly Hills-Mulhol	6.69	13.39
12	960	1994	Northridge	Canyon Country-WLC	6.69	26.49
13	1111	1995	Kobe, Japan	Nishi-Akashi	6.9	8.7
14	1116	1995	Kobe, Japan	Shin-Osaka	6.9	45.97
15	1148	1999	Kocaeli, Turkey	Arcelik	7.51	53.68
16	1158	1999	Kocaeli, Turkey	Duzce	7.51	98.22
17	1244	1999	Chi-Chi, Taiwan	CHY101	7.62	31.96
18	1485	1999	Chi-Chi, Taiwan	TCU045	7.62	77.5
19	1602	1999	Duzce, Turkey	Bolu	7.14	41.27
20	1633	1990	Manjil, Iran	Abbar	7.37	40.43
21	1787	1999	Hector Mine	Hector	7.13	26.53

the tsunami loadings are applied along the transverse direction of the bridge (Y-axis, as shown in Fig. 1), hence the ground motion components with higher earthquake intensity are input along the Y-axis to produce conservative bridge responses. Figure 3 illustrates the acceleration spectra of the selected ground motion records.

### 3.2 Tsunami loadings

Tsunami loadings on the assessed bridge model are computed by a CFD model developed using ANSYS Fluent software, as shown in Fig. 4. Considering the high computational expense for building a complete CFD model, a symmetrical segment of the prototype bridge with a total length of 20m in the longitudinal direction (X-axis, as shown in Fig. 1) is extracted, and is then modelled to study the tsunami-bridge interaction process. The bridge model is treated as a rigid body in the CFD model considering the relatively small allowable deformation in practice. Solitary waves are generated by settling open channel wave boundary conditions at the velocity inlet plane ABCD (Fig. 4). The free surface level method is adopted as the pressure specification and density interpolation methods at the pressure outlet planes EFGH and ABFE (Fig. 4). Other boundary conditions as well as the bridge model surfaces are set as no-slip stationary walls.  $y+$  is a non-dimensional distance, which is often used to describe how coarse or fine a mesh is for the hydrodynamic problem (Ariff et al. 2009). It is important in turbulence modeling to determine the proper size of the cells near domain walls. The  $y+$  values at the grid cells near the bridge deck surfaces are around 50 in the established model.

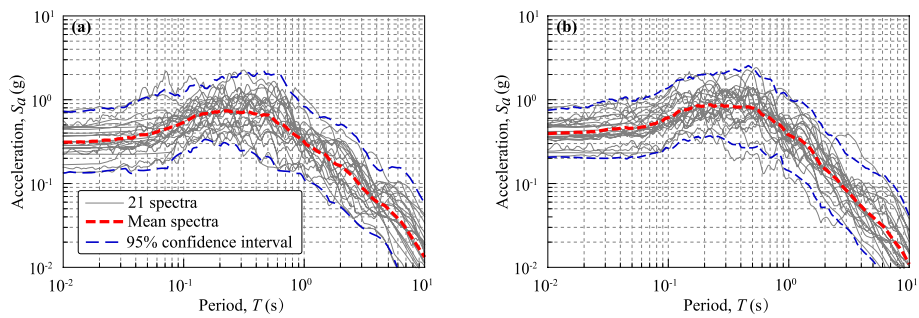


**Fig. 3** Acceleration response spectra of the selected earthquake records: **a** ground motion components along the X-axis and **b** ground motion components along the Y-axis

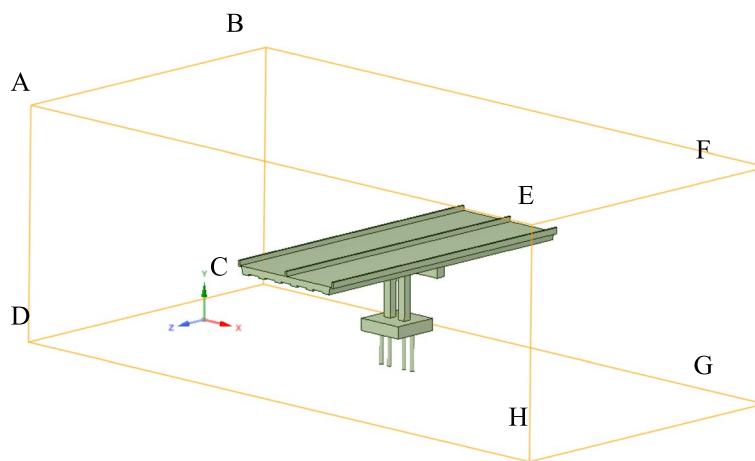


**Fig. 4** CFD numerical model for the tsunami-bridge interaction

In the established CFD model, tetrahedron meshes are utilized to fit the irregular shapes of the girders and diaphragms. Based on the mesh sensitivity analysis results, the mesh size is determined as 0.7 m and the fixed time step is set as 0.0025 s. In addition, the shear stress transport  $k-\omega$  model is adopted and the turbulence damping factor is set as 10. The turbulent intensity of the boundary is set as 2% and the turbulent viscosity ratio is defined as 10%. The pressure-velocity coupling method uses the Pressure-Implicit with Splitting of Operators scheme. The pressure staggering option scheme is set for the pressure spatial discretization, while the least squares cell-based scheme is used for the gradient discretization. More details regarding the CFD-based wave force simulation and its experimental verification can be found in the authors' previous studies (Zhu and Dong 2020; Zhu et al. 2021, 2022; Yuan et al. 2022). In this study, the water depth (D) is 16 m, and five wave height (H) scenarios are defined to examine the effect of this factor on the bridge performance. The lower bound of the wave height is 5 m, in this case the wave force can produce obvious bridge responses. On this basis, the wave height is increased with an increment of 1 m until attains 9 m where the waves swamp the top of the deck. In this manner, five groups of wave force time histories on different structural components are generated for different water height cases, and are applied to the numerical model in OpenSees. Figure 5 shows the schematic diagram of the tsunami

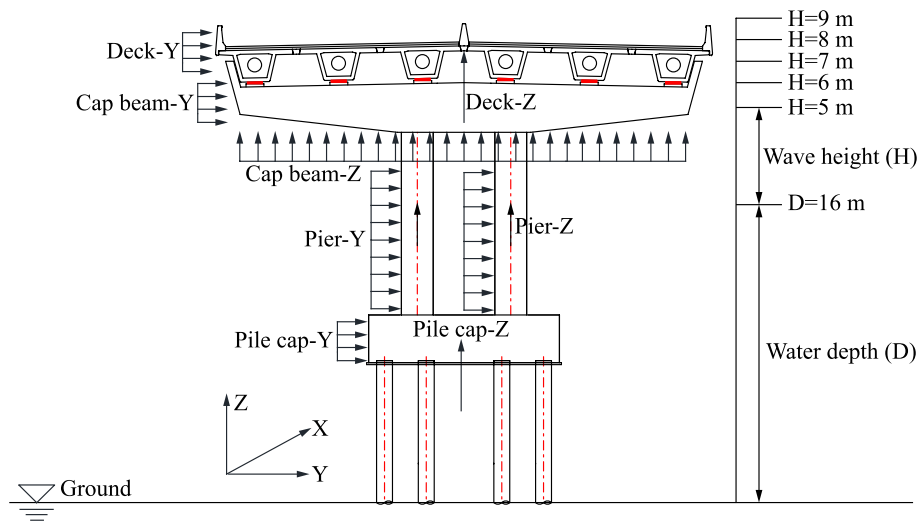


**Fig. 5** Schematic diagram of the tsunami loading application and analysis scenarios

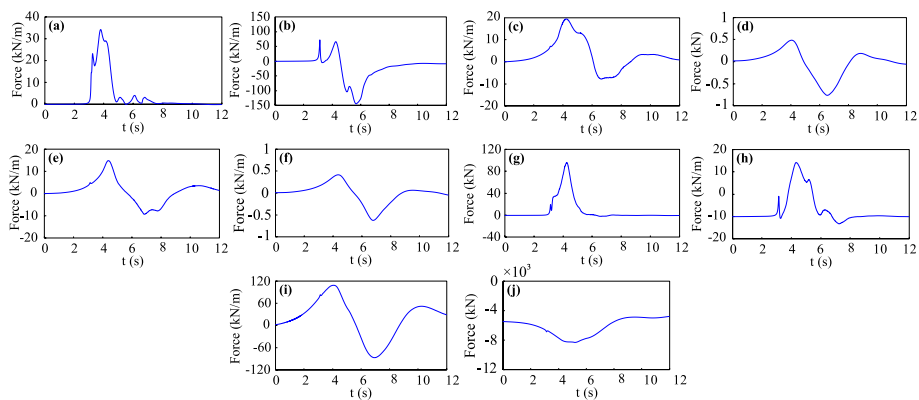


**Fig. 6** Tsunami force time histories of various bridge components under  $D = 16$  m and  $H = 7$  m (“-Y” and “-Z” refer to the loading direction in the global coordinate system): **a** deck-Y, **b** deck-Z, **c** pier P1-Y, **d** pier P1-Z, **e** pier P3-Y, **f** pier P3-Z, **g** cap beam-Y, **h** cap beam-Z, **i** pile cap-Y and **j** pile cap-Z

loading application as well as the analysis scenarios. The case of water depth equal to 16 m and wave height of 7 m is selected to representatively present the patterns of the generated tsunami loadings on various bridge components, as seen in Fig. 6.

### 3.3 Sequential earthquake and tsunami time histories

The earthquake-tsunami sequences start with the earthquake phase, followed by the transient free vibration phase and the tsunami phase. As this study does not account for the correlation between the earthquake and tsunami intensities (i.e., they are mutually independent), each selected ground motion record is separately paired with the generated tsunami loadings. In terms of the free vibration phase, the analysis duration is set as 30 s (Wen et al. 2018) and the time step is assumed as 0.01 s. Through the trial method, this setup is able to guarantee that the bridge stops oscillating before the tsunami phase. On these bases, a total number of 105 (21 ground motion pairs  $\times$  5 groups of tsunami

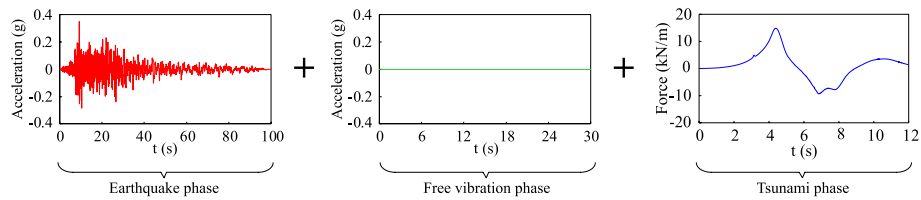


**Fig. 7** Conceptual diagram of the input earthquake-tsunami sequences

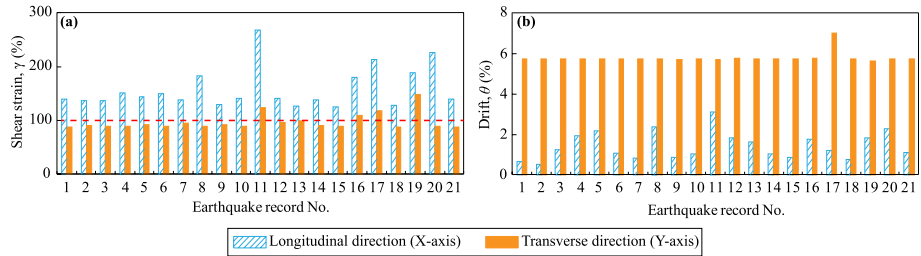


**Fig. 8** Peak responses of bridge components for various earthquake records under  $H=9\text{m}$ : **a** bearing and **b** pier

loading time series) groups of sequential earthquake and tsunami time histories are obtained. Figure 7 illustrates the conceptual diagram of the input sequential earthquake and tsunami time histories in the transverse direction (Y-axis, as shown in Fig. 1).

#### 4 Dynamic bridge performance under earthquake-tsunami sequences

To study the bridge performance under the sequential earthquake and tsunami loadings, the peak horizontal shear strain ( $\gamma$ ) of the rubber bearing and the peak pier drift ( $\theta$ ) in both longitudinal (X-axis) and transverse (Y-axis) directions are adopted as the representative response quantities. Based on the results of responses for various components, the bearing B2 (see Fig. 2) and the pier P1 (see Fig. 2) have the largest demands compared to those of other bearings and piers, respectively, and thereby are taken as the focused components. The analysis results of the bearing B2 and the pier P1 under earthquake-tsunami sequences with different wave heights are shown in the following sections.

##### 4.1 Dynamic responses of bridge components

The scenario of wave height equal to 9 m ( $H=9\text{m}$ ) is selected as the representative case to show the characteristics of the bridge performance under cascading earthquake and tsunami hazards more clearly. Figure 8(a) and (b) illustrate the peak responses of bearings and piers, respectively, for various ground motion records. In terms of the bearings, it can be seen that the longitudinal shear strain (mean value = 159%) is evidently larger than the transverse one (mean value = 97%), and exceeds the empirical damage threshold (100%) (Zhang and Huo 2009). This indicates that the bearings of simply supported girder bridge are more susceptible to the damage in the longitudinal direction than that in the transverse direction. In contrast, the transverse pier drifts are much larger than the longitudinal ones, as shown in Fig. 8(b). More specifically, the average transverse pier

drift is 5.8%, while it turns out to be 1.4% for the longitudinal one. On the other hand, it can be found that the peak transverse pier drift varies slightly across various earthquake records. Hence, it is reasonable to infer that the tsunami loading has a dominant influence on the transverse pier response for this case ( $H=9\text{ m}$ ) due to the constant tsunami input segment for each earthquake-tsunami sequence.

In addition, previous studies uncover the occurrence of shear failure in the bridge pier under the tsunami loadings, and emphasize the significance of this failure mode to the safety of the whole bridge (Xu et al. 2021a, b). For this purpose, the peak shear forces at the pier bottom for various earthquake-tsunami sequences are obtained, as shown in Fig. 9. It can be observed that the transverse shear forces are visibly larger than the longitudinal ones. Similar to the transverse pier drift in Fig. 8(b), there are small differences in the peak shear force among various sequences with the dispersion of 0.016, which signifies that the tsunami loadings contribute more to the shear demand of piers as compared to the seismic excitations. Despite of the non-negligible shear responses, it can be indicated from Fig. 9 that the pier does not sustain the shear failure because of the high shear strength (14,393.6 kN).

#### 4.2 Effects of preceding earthquakes and wave heights on the bridge performance

Previous studies confirm that the preceding earthquake and the wave height affect the structural performance (Xu et al. 2021b). To examine the impact of this factor on the behavior of the simply supported girder bridges, the demand ratios for the studied components are defined, which are calculated through the peak response under the earthquake-tsunami sequence divided by that under the corresponding tsunami loading phase only. The spectral acceleration at the first natural vibration period ( $S_{a,T_1}$ ), which is verified as a suitable intensity measure (IM) for the performance assessment of regular girder bridges in previous studies (Gardoni et al. 2009; Gardoni and Rosowsky 2011; Zhong et al. 2012; Carey et al. 2019), is taken as the IM to identify the variability of demand ratio with respect to the earthquake intensity.

Figures 10 and 11 illustrate the longitudinal and transverse bearing shear strain ratios (notated as  $\gamma_{L(EQ-TS)}/\gamma_{L(TS)}$  and  $\gamma_{T(EQ-TS)}/\gamma_{T(TS)}$ , respectively), respectively, with respect to the  $S_{a,T_1}$  under different wave heights. It can be seen from Figs. 10 and 11 that the

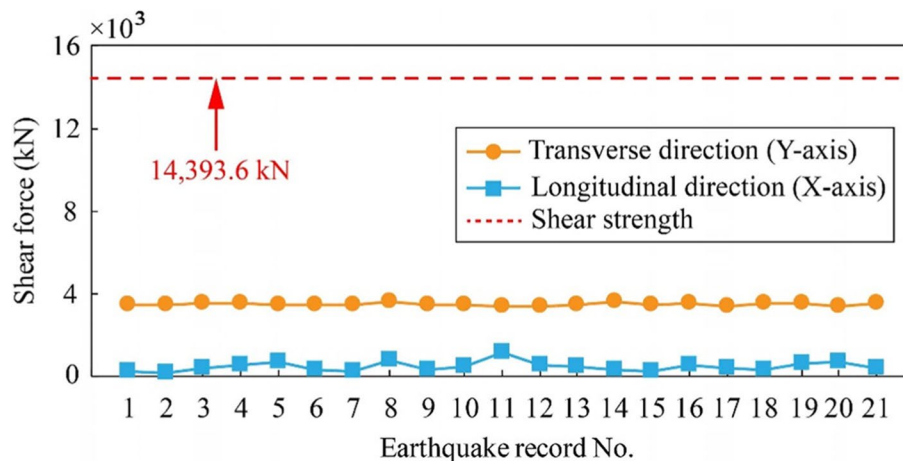
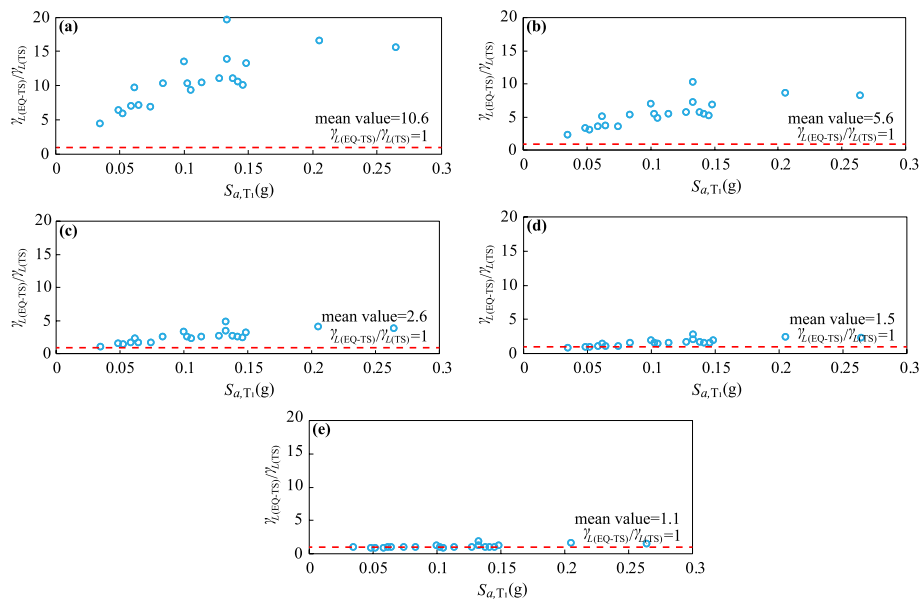


Fig. 9 Peak shear force at the pier bottom for various earthquake records under  $H=9\text{ m}$



**Fig. 10** Ratio of longitudinal bearing shear strain with respect to the  $S_{a,T_1}$  under the wave height (H) of: **a** 5 m, **b** 6 m, **c** 7 m, **d** 8 m and **e** 9 m

preceding earthquakes have a significant effect on the bearing shear strain because most of the demand ratios are more than 1 under different wave heights, which implies that involving the preceding ground motions can induce larger responses compared to discarding them. Notably, this effect becomes pronounced with the increase of seismic intensity. Compared with the longitudinal bearing responses, the preceding earthquakes contribute more to the transverse ones, with larger average shear strain ratio under the same wave height. Moreover, it can also be observed that both the longitudinal and transverse shear strain ratios approach 1 with the increase of wave heights, which signifies that the importance of preceding earthquakes to the bearing responses reduces as the effect of tsunami wave forces rises caused by the increasing wave height.

Figures 12 and 13 show the longitudinal and transverse pier drift ratios (notated as  $\theta_{L(EQ-TS)}/\theta_{L(TS)}$  and  $\theta_{T(EQ-TS)}/\theta_{T(TS)}$ , respectively), respectively, with respect to the  $S_{a,T_1}$  under different wave heights. It can be reported from Fig. 12 that the preceding earthquakes have a noticeable effect on the longitudinal pier drift because of the high drift ratios, even for the case of wave height equal to 9 m that has an average drift ratio of 7.2. Similar to the bearing cases, the drift ratios become higher with the increasing  $S_{a,T_1}$  under the same wave height, which indicates that the impact of preceding earthquakes increases as the ground motion intensity rises. The above phenomena are mainly owing to the fact that only earthquake loadings are applied along the longitudinal direction of the bridge, and thereby dominate the pier drifts in this direction.

Compared to the longitudinal pier drift, it can be seen from Fig.13 that the preceding ground motions have a smaller impact on the transverse pier drift. In particular, the drift ratios vary slightly and decrease to around 1 when the wave height is higher than 7 m. This observation demonstrates that the tsunami loadings become dominant for the transverse pier response under higher wave heights, which is consistent with the results in Fig. 8(b).

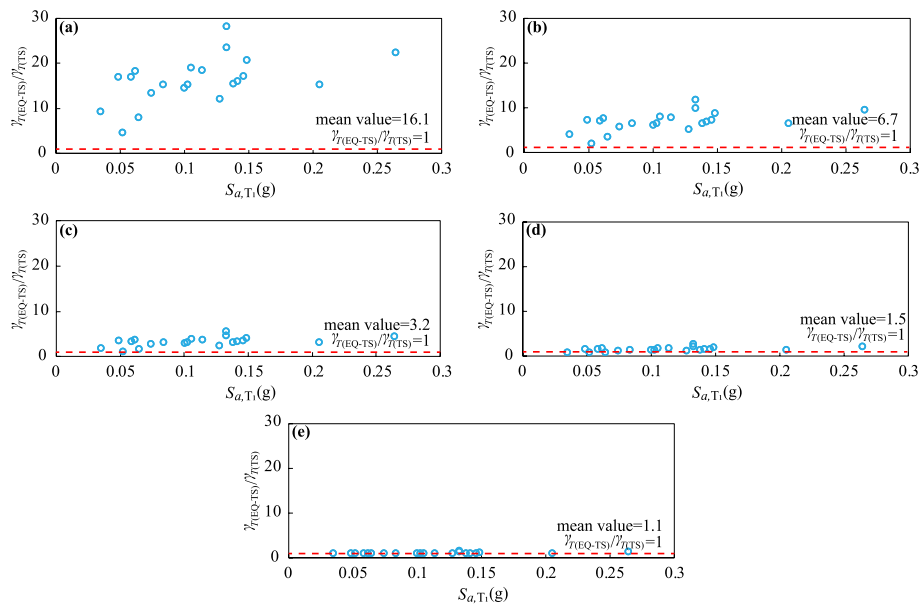


**Fig. 11** Ratio of transverse bearing shear strain with respect to the  $S_{a,T_1}$  under the wave height (H) of: **a** 5 m, **b** 6 m, **c** 7 m, **d** 8 m and **e** 9 m

### 5 Conclusions

This paper assesses the performance of simply supported girder bridges under the sequential earthquake and tsunami loadings. A three-span simply supported concrete girder bridge is investigated as an illustrative example. Then, a set of 21 pairs of earthquake records are selected, and 5 refined tsunami force time series are generated based on an advanced three-dimensional CFD model. In this manner, 105 (i.e.,  $21 \times 5$ )

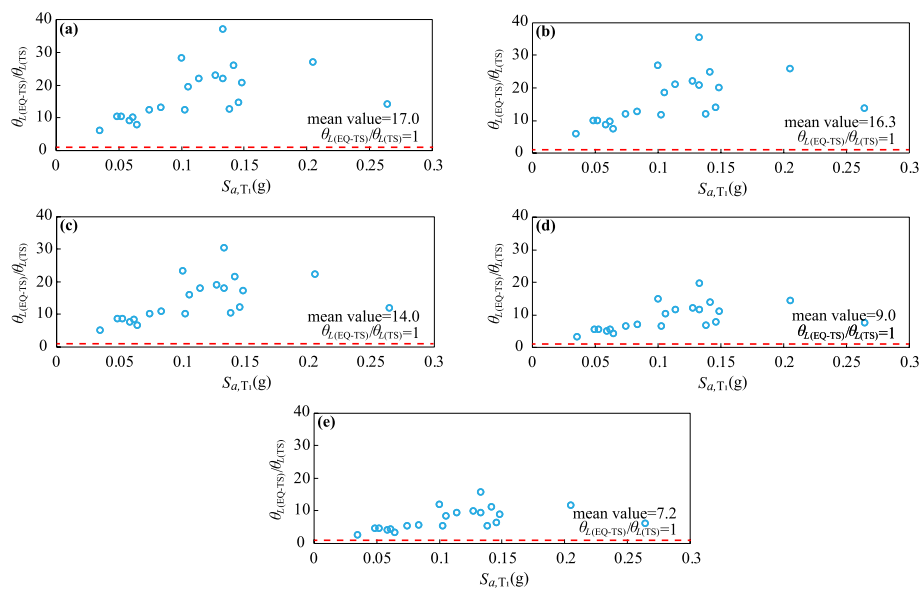


**Fig. 12** Ratio of longitudinal pier drift with respect to the  $S_{a,T_1}$  under the wave height (H) of: **a** 5 m, **b** 6 m, **c** 7 m, **d** 8 m and **e** 9 m

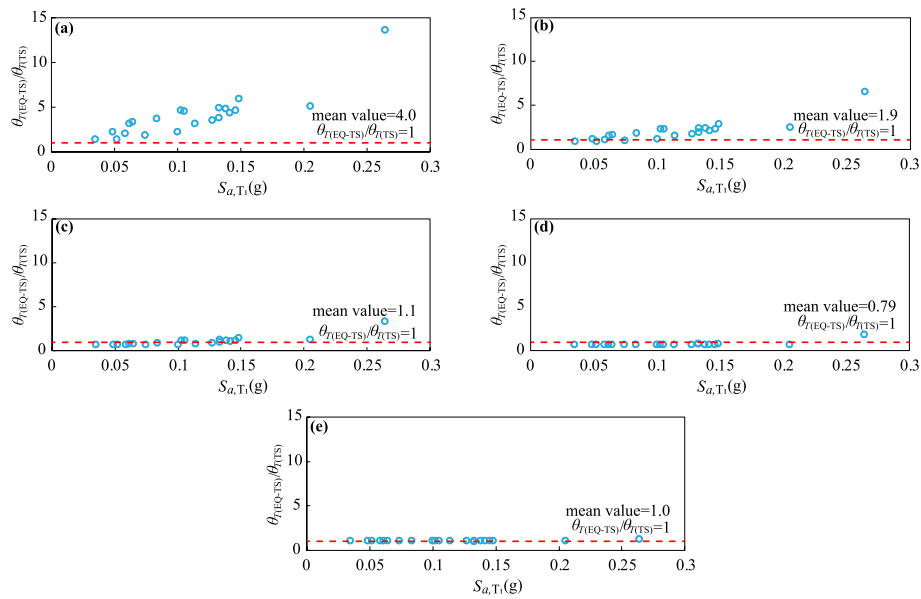


**Fig. 13** Ratio of transverse pier drift with respect to the  $S_{a,T_1}$  under the wave height (H) of: **a** 5 m, **b** 6 m, **c** 7 m, **d** 8 m and **e** 9 m

groups of earthquake-tsunami loading time histories are formed. Subsequently, the dynamic performance (e.g., pier drift, bearing shear strain) of the case-study bridge subjected to the successive earthquake and tsunami loadings is studied. Finally, the effects of the preceding earthquakes and the wave height on the bridge performance are explored. The main conclusions are drawn as below:

- (1) The bearings sustain more damage in the longitudinal direction than that in the transverse direction. For the case-study bridge under the tsunami wave height of 9 m, the average longitudinal shear strain under different earthquake-tsunami sequences is 159%, whereas the transverse one is 97%. By comparison, the transverse pier responses are much larger than the longitudinal ones. For the scenarios of wave height equal to 9 m, the average transverse pier drift is 5.8%, while the average longitudinal pier drift is 1.4%.
- (2) The transverse shear forces at the pier bottom are significantly larger than the longitudinal ones. Due to the high shear strength of the pier, the case-study bridge is not subjected to the shear failure. Compared to the seismic excitation, the tsunami loadings contribute more to the shear demand of piers.
- (3) The preceding earthquakes have a significant effect on the bearing shear strain and longitudinal pier drift, and the effect becomes more pronounced with the increase of seismic intensity. In contrast, the preceding ground motions have a smaller impact on the transverse pier drift.
- (4) The contribution of the tsunami loadings to the bridge response increases as the wave height rises. As a result, the demand ratios of bearings and piers approach 1 with the increasing wave heights. In particular, the tsunami loadings become dominant for the transverse pier drift when the wave height is higher than 7 m.

**Acknowledgements**

The authors gratefully acknowledge Dr. Xiaowei Wang for the support in terms of the wave force application in OpenSees.

**Authors' contributions**

Ruiwei Feng: Methodology, Software, Validation, Formal analysis, Investigation, Data curation, Writing - original draft, Writing - review & editing, Visualization. Deming Zhu: Methodology, Software, Validation, Investigation, Data curation, Writing - original draft. You Dong: Conceptualization, Methodology, Writing - review & editing, Supervision, Project administration, Funding acquisition. All authors have read and approved the manuscript.

**Funding**

The study has been supported by the Research Institute for Sustainable Urban Development, the Hong Kong Polytechnic University (Grant No. PolyU1-BBWM), National Natural Science Foundation of China (grant nos. 52078448) and the Research Grant Council of Hong Kong (project no. PolyU 15221521 and PolyU 15219819). The support is gratefully acknowledged. The opinions and conclusions presented in this paper are those of the authors and do not necessarily reflect the views of the sponsoring organizations.

**Availability of data and materials**

No other data sources need to be provided and no data will be shared.

**Declarations****Competing interests**

The authors declare that they have no known competing financial interests or personal relationships that could have appeared to influence the work reported in this paper.

Received: 8 June 2022 Accepted: 30 July 2022

Published online: 01 September 2022

**References**

- Akiyama M, Frangopol DM (2014) Reliability of bridges under seismic and tsunami hazards. In: *Vulnerability, uncertainty, and risk*. American Society of Civil Engineers, Reston, pp 1696–1705
- Ariff M, Salim S M, & Cheah S C (2009). Wall y+ approach for dealing with turbulent flow over a surface mounted cube: part 2—high Reynolds number. In: *The seventh international conference on CFD in the minerals and process industries CSIRO, Melbourne, Australia (Vol. 9, No. 11)*
- ATC (2008) Quantification of building seismic performance factors. FEMA P695, Washington, DC
- Attary N, Van De Lindt JW, Barbosa AR, Cox DT, Unnikrishnan V (2021) Performance-based tsunami engineering for risk assessment of structures subjected to multi-hazards: tsunami following earthquake. *J Earthq Eng* 25:2065–2084
- Carey TJ, Mason HB, Barbosa AR, Scott MH (2019) Multihazard earthquake and tsunami effects on soil–foundation–bridge systems. *J Bridg Eng* 24:04019004
- Clague JJ, Munro A, Murty T (2003) Tsunami hazard and risk in Canada. *Nat Hazards* 28:435–463
- FEMA (2012) Guidelines for design of structures for vertical evacuation from tsunamis. FEMA P-646, Washington, DC
- Feng R, Wang X, Yuan W, Yu J (2018) Impact of seismic excitation direction on the fragility analysis of horizontally curved concrete bridges. *Bull Earthq Eng* 16:4705–4733
- Feng R, Yuan W, Sextos A (2021) Probabilistic loss assessment of curved bridges considering the effect of ground motion directionality. *Earthq Eng Struct Dyn* 50:3623–3645
- Gardoni P, Mosalam K, Der Kiureghian A (2009) Probabilistic seismic demand models and fragility estimates for RC bridges. *J Earthq Eng* 7:79–106
- Gardoni P, Rosowsky D (2011) Seismic fragility increment functions for deteriorating reinforced concrete bridges. *Struct Infrastr Eng* 7:869–879
- Gautam D, Dong Y (2018) Multi-hazard vulnerability of structures and lifelines due to the 2015 Gorkha earthquake and 2017 central Nepal flash flood. *J Build Eng* 17:196–201
- Gidaris I, Padgett JE, Barbosa AR, Chen S, Cox D, Webb B, Cerato A (2017) Multiple-hazard fragility and restoration models of highway bridges for regional risk and resilience assessment in the United States: state-of-the-art review. *J Struct Eng* 143:04016188
- Goda K, De Risi R, De Luca F, Muhammad A, Yasuda T, Mori N (2021) Multi-hazard earthquake-tsunami loss estimation of Kuroshio town, Kochi prefecture, Japan considering the Nankai-Tonankai megathrust rupture scenarios. *Int J Disaster Risk Reduct* 54:102050
- Goda K, Li S, Mori N, Yasuda T (2015) Probabilistic tsunami damage assessment considering stochastic source models: application to the 2011 Tohoku earthquake. *Coast Eng J* 57:1550015–1–1550015–38
- Ji D, Wen W, Zhai C, Lu D (2021) Inelastic displacement ratios for SDOF structures subjected to earthquake-tsunami loadings. *J Earthq Eng* 00:1–19
- LeBorgne MR, Ghannoum WM (2014) Calibrated analytical element for lateral-strength degradation of reinforced concrete columns. *Eng Struct* 81:35–48
- Mander JB, Priestley MJN, Park R (1988) Theoretical stress-strain model for confined concrete. *J Struct Eng* 114:1804–1826
- Mangalathu S, Heo G, Jeon J-S (2018) Artificial neural network based multi-dimensional fragility development of skewed concrete bridge classes. *Eng Struct* 162:166–176
- McKenna F (2011) OpenSees: a framework for earthquake engineering simulation. *Comput Sci Eng* 13:58–66

- MOT (Ministry of Transport) (2007). Series of elastomeric pad bearings for highway bridges (JT/T 663-2006), Beijing
- MOT (Ministry of Transport) (2018). Specification for design of highway reinforced concrete and prestressed concrete bridges and culverts (JTG/T 3362-2018), Beijing
- MOT (Ministry of Transport) (2020). Specifications for seismic design of highway bridges (JTG/T 2231-01-2020), Beijing
- Muthukumar S, DesRoches R (2006) A hertz contact model with non-linear damping for pounding simulation. *Earthq Eng Struct Dyn* 35:811–828
- Nielson BG (2005) Analytical fragility curves for highway bridges in moderate seismic zones. Ph.D. Thesis, Georgia Institute of Technology, Atlanta, GA, 2005
- Park S, van de Lindt JW, Cox D, Rakesh G, Aguiniga F (2012) Successive earthquake-tsunami analysis to develop collapse fragilities. *J Earthq Eng* 16:851–863
- Petrone C, Rossetto T, Baiguera M, Bustamante C, Ioannou I (2020) Fragility functions for a reinforced concrete structure subjected to earthquake and tsunami in sequence. *Eng Struct* 205:110120
- Priestley MJN, Verma R, Xiao Y (1994) Seismic shear strength of reinforced concrete columns. *J Struct Eng* 120:2310–2329
- Rossetto T, De la Barra C, Petrone C, De la Llera JC, Vásquez J, Baiguera M (2019) Comparative assessment of nonlinear static and dynamic methods for analysing building response under sequential earthquake and tsunami. *Earthq Eng Struct Dyn* 48(8):867–887
- Salem H, Mohssen S, Nishikiori Y, Hosoda A (2016) Numerical collapse analysis of Tsuyagawa bridge damaged by Tohoku tsunami. *J Perform Constr Facil* 30:04016065
- Sugimoto T, Unjoh S (2007) Hydraulic model tests on the bridge structures damaged by tsunami and tidal wave. Proc 23rd US-Japan Bridge Eng Work, pp 233–242
- Tagle SJ, Jünemann R, Vásquez J, de la Llera JC, Baiguera M (2021) Performance of a reinforced concrete wall building subjected to sequential earthquake and tsunami loading. *Eng Struct* 238:111995
- Taucer FF, Spacone E, Filippou FC (1991) A fiber beam-column element for seismic response analysis of reinforced concrete structures. Earthquake Engineering Research Center, College of Engineering, University of California, Berkeley
- Tu B, Dong Y, Fang Z (2019) Time-dependent reliability and redundancy of corroded prestressed concrete bridges at material, component, and system levels. *J Bridge Eng* 24(9):04019085-1-14
- Wen W, Ji D, Zhai C, Li X, Sun P (2018) Damage spectra of the mainshock-aftershock ground motions at soft soil sites. *Soil Dyn Earthq Eng* 115(April):815–825
- Xu J-G, Feng D-C, Wu G (2021a) Life-cycle performance assessment of aging bridges subjected to tsunami hazards. *J Bridge Eng* 26:04021025
- Xu J-G, Wu G, Feng D-C, Fan J-J (2021b) Probabilistic multi-hazard fragility analysis of RC bridges under earthquake-tsunami sequential events. *Eng Struct* 238:112250
- Yuan P, Zhu D, Dong Y, Xu G (2022) Response-based bridge deck limit state considering component-level failure under extreme wave. *Mar Struct* 83:103184
- Zhang J, Huo Y (2009) Evaluating effectiveness and optimum design of isolation devices for highway bridges using the fragility function method. *Eng Struct* 31:1648–1660
- Zhong J, Gardoni P, Rosowsky D (2012) Seismic fragility estimates for corroding reinforced concrete bridges. *Struct Infrastruct Eng* 8:55–69
- Zhu D, Dong Y (2020) Experimental and 3D numerical investigation of solitary wave forces on coastal bridges. *Ocean Eng* 209:107499
- Zhu D, Dong Y, Frangopol DM (2022) Experimental and numerical investigation on wave impacts on box-girder bridges. *Struct Infrastruct Eng* 0:1–19
- Zhu D, Yuan P, Dong Y (2021) Probabilistic performance of coastal bridges under hurricane waves using experimental and 3D numerical investigations. *Eng Struct* 242:112493

## Publisher's Note

Springer Nature remains neutral with regard to jurisdictional claims in published maps and institutional affiliations.

Submit your manuscript to a SpringerOpen<sup>®</sup> journal and benefit from:

- Convenient online submission
- Rigorous peer review
- Open access: articles freely available online
- High visibility within the field
- Retaining the copyright to your article

---

Submit your next manuscript at ► [springeropen.com](https://www.springeropen.com)

---